

A uniaxial bioMEMS device for quantitative force-displacement measurements

David B. Serrell · Tammy L. Oreskovic ·
Andrew J. Slifka · Roop L. Mahajan · Dudley S. Finch

Published online: 23 December 2006
© Springer Science + Business Media, LLC 2007

Abstract There is a need for experimental techniques that allow the simultaneous imaging of cellular cytoskeletal components with quantitative force measurements on single cells. A bioMEMS device has been developed for the application of strain to a single cell while simultaneously quantifying its force response. The prototype device presented here allows the mechanical study of a single, adherent cell *in vitro*. The device works in a fashion similar to a displacement-controlled uniaxial tensile machine. The device is calibrated using an AFM cantilever and shows excellent agreement with the calculated spring constant. The device is demonstrated on a single fibroblast. The force response of the cell is seen to be linear until the onset of de-adhesion with the de-adhesion from the cell platform occurring at a force of approximately 1500 nN.

Keywords Cell mechanics · BioMEMS · Fibroblast · Microfabrication · De-adhesion

Introduction

Recent evidence in the literature shows the importance of mechanical forces on cellular function and behavior. Me-

chanical stresses on cells can influence a variety of cellular processes such as growth, differentiation, apoptosis, contraction, division, spreading and the regulation of protein transduction (Chicurel et al., 1998; Janmey, 1998; Maniotis et al., 1997). Furthermore, several well-known pathologies such as sickle cell anemia and asthma are related to the mechanical properties of cells. Despite the importance of forces on cell life, the underlying mechanisms for how these forces are transmitted and regulated within living cells are poorly understood.

There are a wide variety of techniques available to quantify mechanical forces on single cells *in vitro*. Techniques such as atomic force microscopy (Florin et al., 1994; Hyonchol et al., 2002; Mathur et al., 2001; Yamamoto et al., 1998), magnetic traps (Alenghat et al., 2000; Chen et al., 2001; Lo et al., 1998; Wang et al., 1993), optical traps (Svoboda and Block, 1994; Yamada et al., 2000) and silicon cantilevers (Saif et al., 2003, 2002) have been used for studying local cellular phenomena as well as individual components of the cytoskeleton such as actin (Minajeva et al., 2001; Zaner and Valberg, 1989). However, studying local phenomena and individual cytoskeletal components through these techniques is of limited use since cells exhibit different mechanical behavior at the local and global levels (Fabry et al., 2001; Fabry et al., 2003). Recent advances in imaging techniques have allowed investigators to study the architecture of cellular structure in great detail. Integrating these imaging techniques into functioning mechanical experiments has proven challenging. Experimental protocols focused on quantifying forces on single cells and simultaneously imaging those cells at a macroscopic level have the potential to provide new insights into the relationship between forces and structure.

Techniques used to study single-cell mechanics at the macroscopic level include micropipette aspiration (Evans

D. B. Serrell (✉) · T. L. Oreskovic · A. J. Slifka · D. S. Finch
National Institute of Standards and Technology,
Boulder, CO, USA
e-mail: serrell@colorado.edu

D. B. Serrell · R. L. Mahajan
University of Colorado,
Boulder, CO, USA

R. L. Mahajan
University of Virginia Technology,
Blacksburg, VA, USA

and Yeung, 1989; Evans and Hochmuth, 1976; Hochmuth, 1981; Hochmuth and Waugh, 1987), flexible silicon substrates (Di Palma et al., 2003; Ignatius et al., 2004; Moretti et al., 2004; Park et al., 2004), shear flow devices (Ainslie et al., 2005; Rhodes et al., 1998; Soghomonians et al., 2005), glass microplates (Desprat et al., 2005; Thoumine and Ott, 1997) and silicon cantilevers (Yang and Saif, 2005). While each of these techniques has strengths and limitations, none is specifically designed to correlate mechanical data with cytoskeletal morphology. An ideal technique would allow for a variety of cellular interventions to be performed on an adherent cell. Extracellular forces, such as chemical pathogens or applied strain, and intracellular forces, such as genetic mutations, could be provided as an input. A mutation in any of the genes responsible for the formation of known structural proteins, such as actin or collagen, can cause those proteins to lose functionality and alter the strength of the cell. The output of such a device would not only provide quantitative data in the form of force information but qualitative data in the form of real-time images of the cytoskeleton. Furthermore, mechanical stimulation or measurement would occur through the focal adhesion complexes to simulate the true physiological state of the cell *in vivo*. Traditionally, the mechanical testing of single cells has focused on the bilipid cell membrane properties and ignored the role of internal structures (Fung and Liu, 1993; Schmid-Schonbein et al., 1981). Focal adhesion complexes, containing the transmembrane integrin adhesion molecules, mechanically link the extra cellular matrix to the internal structural components of the cell such as actin and other cytoskeletal elements. By imaging these focal adhesion sites, the effective area of adhesion can be quantified, greatly aiding in the testing of de-adhesion protocols and allowing for a stress to be reported rather than a force value. Furthermore, mechanical forces could be correlated to changes in internal structure.

This paper describes the prototype of a novel, microfabricated device designed to measure the mechanical properties of an entire, adherent single cell while simultaneously allowing imaging of the cell. The current prototype presented here stands as a proof-of-principle for the biological feasibility of such a device although the transparent substrate required for imaging is not yet present in this design. In this device, microactuators and microsensors are used to quantify and manipulate a single cell. The operation of the device is described as well as the actuation and sensing techniques used. The sensor is calibrated using an AFM cantilever. To demonstrate the device, a single fibroblast is placed on the cell platform and its force response to an applied displacement is measured. Cell culturing and placement techniques are also described.

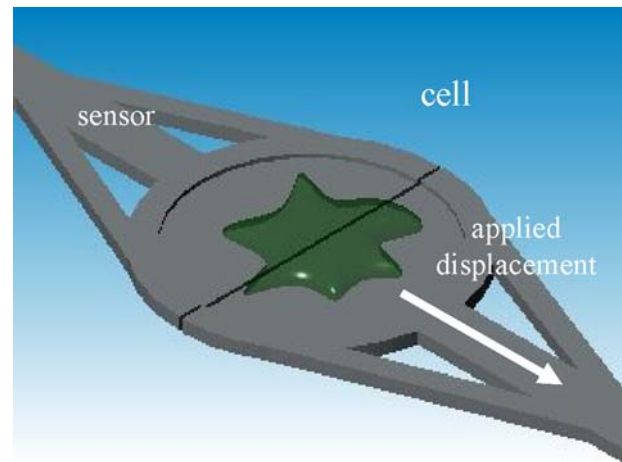


Fig. 1 Basic concept of the cell tensometer

Methods

Cell puller

In this section, the design and fabrication of the device is described. An actuation mechanism was selected that provides large, linear displacements and is compatible with an aqueous and highly ionic cell solution. The sensor resolves cell-level forces and is compatible with immersion in the cell culture media.

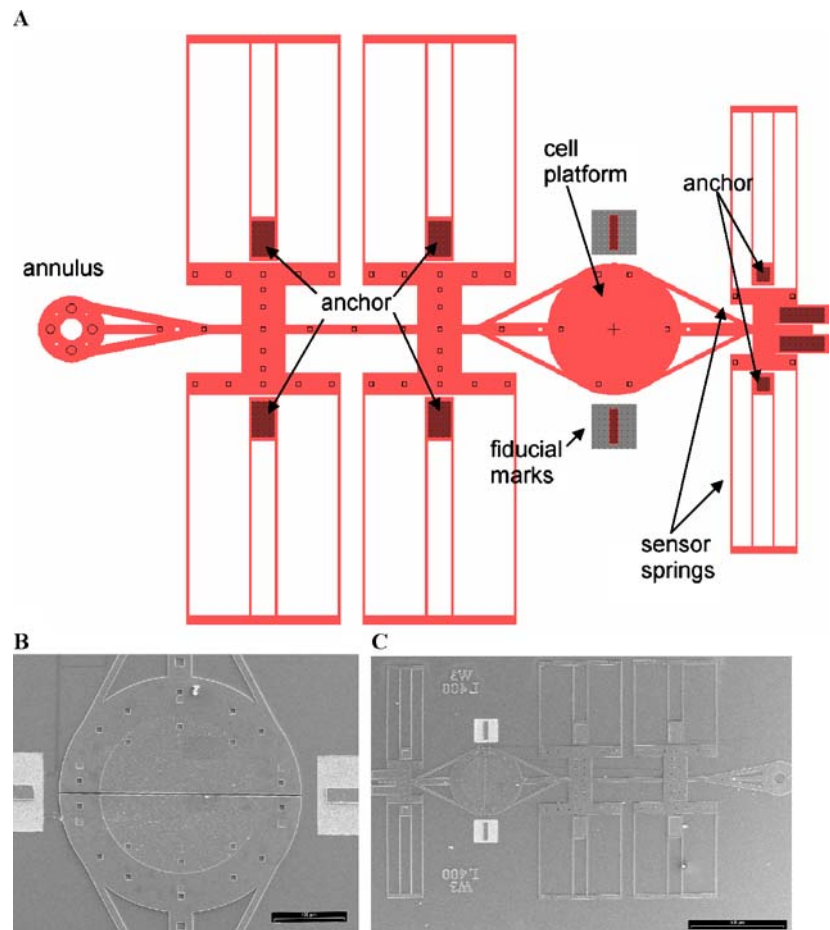
The function of the device revolves around a single-cell platform (Fig. 1) that is circular and divided in two parts. A cell is placed on the platform and allowed to adhere after which a displacement is applied to one half of the cell platform while the other half is mechanically linked to a sensor that can measure the force on the cell. The actuation is provided by an off-chip micromanipulator while the sensor is a series of cantilever beams. The device works in a similar fashion to a displacement-controlled uniaxial tensile machine.

Actuation

Rather than using an electrostatic comb-type actuator or a thermal actuator, a simple design employing a ring that can be hooked by a probe-station tip was developed to enable rapid prototyping and to test the biological feasibility of the device. This actuation technique allows for displacements large enough to provide for de-adhesion-type experiments in which the cell can withstand as much as 25% strain before deadhering. Smaller strains applied cyclically are also useful for long-term studies of mechanical strain as an input parameter.

The actuator is attached to the cell platform by a polysilicon beam supported by several folded-beam cantilever

Fig. 2 CAD layout of the cell tensometer (A) and SEM pictures of the fabricated device (B,C)



springs (Fig. 2). A standard probe tip is inserted into an annulus at the end opposite the cell platform. A commercially available, off-chip manipulator is used to provide the necessary displacement with a resolution of 40 nm. The actuator has the ability to produce large displacements limited only by spring geometry. The maximum displacement of the actuator is 100 μm . The frequency of actuation is a function of the mass and stiffness of the system. The mass of the micromanipulator is much greater than that of the polysilicon device. Therefore, the actuation frequency is dominated by the micromanipulator. According to the manufacturer, the manipulator is capable of 240 Hz. Unlike other types of actuation requiring electricity to drive them, this device does not need to be isolated from the cell environment; thus, no specialized packaging is required.

Force sensing

The sensing side of the device is based on a series of cantilever beams arrayed in series and parallel to create a spring (Fig. 2). By designing the springs with a known spring constant and measuring displacement of the sensor side of the cell platform, the force on the cell can be

measured. Many of the same advantages for the actuator apply for the sensor, such as ease of design and simple packaging.

The displacement of the cell platform is measured using a high-speed, high-resolution camera. Individual images of the cell experiments are captured at a rate of up to three frames per second. The images are converted to their corresponding gray scale and density-sliced with square etch holes in the suspended polysilicon structures used as reference points in each image. Fiducial marks are etched into the substrate wafer and remain stationary. The centers of the etch holes in the suspended polysilicon structures are then defined mathematically. The change in distance between the centers of the moving polysilicon features and the stationary fiducial marks is then calculated from image to image. Using this technique, we estimate the resolution of the displacement measurement to be 50 nm.

The spring constant of the folded-beam springs can be calculated using standard beam theory. Each folded beam is composed of two types of beams: a long beam (L_1) and a short beam (L_2). The equation of a standard cantilevered beam can be found for both beam types that make up the folded cantilever beam (Fig. 3(A)):

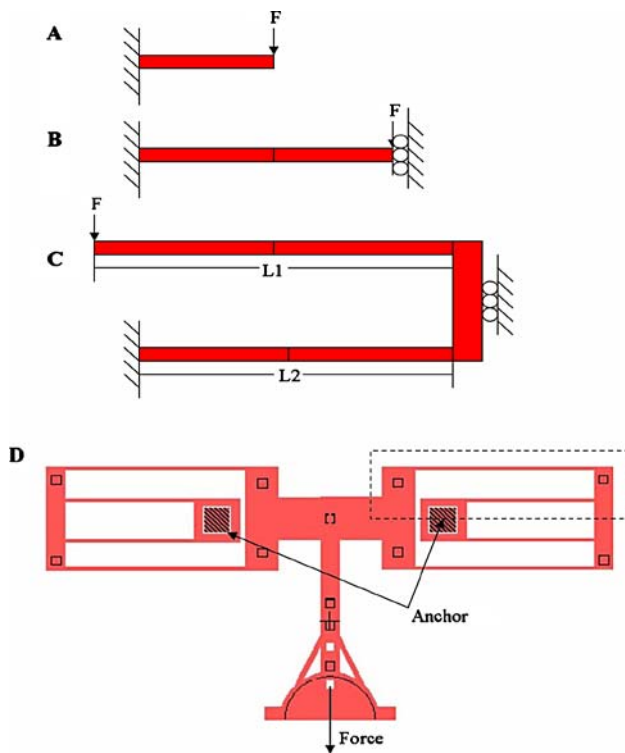


Fig. 3 The spring constant of the folded-beam assembly is calculated by first taking a single cantilevered beam (A) and arraying it in series (B) with an identical beam. The free end of the folded-beam can be modeled as a roller support. These two beams are then in series with the beams fixed to the other end of the roller support (C). There are a total of four of these assemblies in parallel (indicated by the dashed box) for the entire spring

$$k_{L_1/2} = \frac{3EI}{(L_1/2)^3} = \frac{2Ehw^3}{L_1^3} \quad (1)$$

$$k_{L_2/2} = \frac{3EI}{(L_2/2)^3} = \frac{2Ehw^3}{L_2^3} \quad (2)$$

$$I = \frac{hw^3}{12} \quad (3)$$

where E is Young's Modulus, I is moment of inertia (Lardner and Archer, 1994), L_1 and L_2 are the beam lengths, h is the depth of the beam and w is the width. Each of these spring constants represents half of the beam. The entire beam consists of two cantilevered beams in series (Fig. 3(B)):

$$k_{L_1} = \frac{k_{L_1/2}}{2} \quad (4)$$

$$k_{L_2} = \frac{k_{L_2/2}}{2} \quad (5)$$

These two beams are in series with each other (through the guided end support) (Fig. 3(C)). Four of these beam

assemblies make up the entire spring mechanism each in parallel with each other giving a final spring constant of (Fig. 3(D)):

$$k_{\text{spring}} = 4 \left(\frac{2}{k_{L_1/2}} + \frac{2}{k_{L_2/2}} \right)^{-1} = 4Ew^3h \left(\frac{1}{L_1^3} + \frac{1}{L_2^3} \right) \quad (6)$$

The fabrication process of the springs largely dictates the viability of such fine spring structures. Using the current process, beams as thin as $2 \mu\text{m}$ are possible but the yield of defect free samples is low ($< 20\%$). Beams with a width of $3 \mu\text{m}$ and with lengths $L_1 = 500 \mu\text{m}$ and $L_2 = 443 \mu\text{m}$ can be fabricated more reliably and are easily released. These are the limiting design parameters for the springs.

Sensor calibration

The in-plane stiffness of the sensor springs is dictated by Eq. (6) shown above. The primary uncertainty in the calculation of k is the geometry of the beams. By the nature of the deposition process, the thickness of the beams themselves can vary from chip to chip. Therefore, the springs were calibrated using a commercially available silicon AFM cantilever. The AFM cantilever was a "tip less" design and had been previously calibrated by the manufacturer (Tortonese and Maruyama, 1997).

The AFM cantilever was mounted on a custom-made fixture that allowed it to be placed with a micromanipulator in proximity to the springs on the chip. The free end of the AFM cantilever was put in contact with one side of the spring (Fig. 4(A)) at the working angle recommended by the manufacturer (12.5° from vertical). A motorized stage was then used to move the chip in one micron increments and images were taken of each successive movement. By using this technique, the displacement of the spring and the displacement of the chip relative to the AFM cantilever can both be seen in each frame. F_1 is the force on the entire spring system and F_2 is the force on the sensor springs:

$$F_1 = \left(\frac{1}{k_{\text{spring}}} + \frac{1}{k_{\text{AFM}}} \right)^{-1} * d \quad (7)$$

$$F_2 = k_{\text{spring}} * d_1 \quad (8)$$

where k_{spring} is the spring constant of the sensor spring, k_{AFM} is that for the AFM cantilever and d is the displacement of the chip relative to the stationary AFM tip. F_2 is the force on the sensor spring where d_1 is the displacement of that spring. From a free body diagram, the forces on each spring must be equal and the two equations can be set equal to each other.

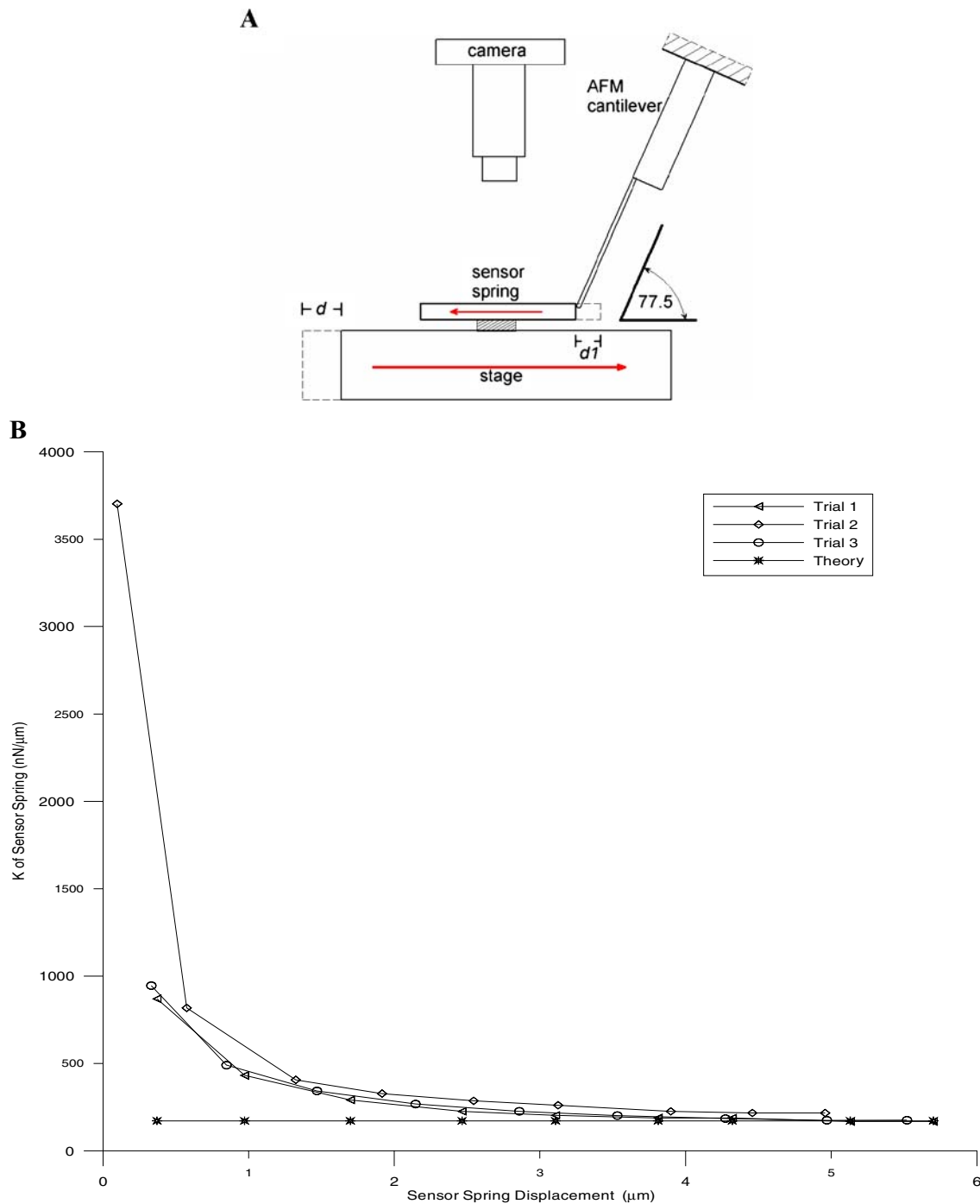


Fig. 4 The calibration setup using a tipless AFM cantilever (A). The stage is moved relative to the stationary AFM tip a distance d , resulting in displacement d_1 of the sensor spring. The stage is moved in one

micron increments and images of each step are captured. The displacements are then calculated from the images. Calibration curves shown converging on theoretical value (B)

Solving for k_{spring} yields:

$$k_{\text{spring}} = \frac{(d - d_1) * k_{\text{AFM}}}{d_1} \tag{9}$$

The primary uncertainty in the calibration occurs when the AFM cantilever makes contact with the spring. Typically,

there is a small gap between the tip and the spring that is not visible through the fluid meniscus. This gap creates artificially high spring constants at the onset of the experiment. However, when extrapolated, the results converge to a single value (Fig. 4(B)). The calibrated spring constant for the average of three runs was found to be $185.80 \pm 24.31 \text{ nN}/\mu\text{m}$. The actual dimensions of the spring were measured opti-

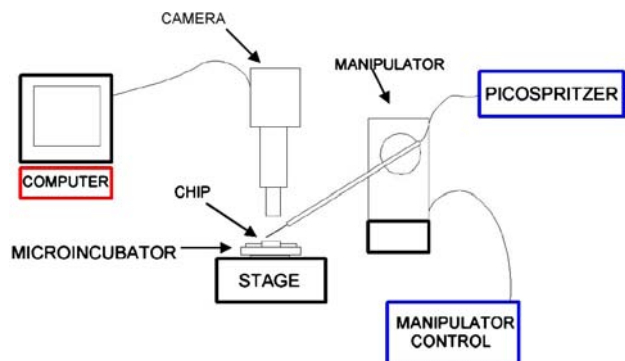


Fig. 5 A probe station has been modified to accommodate all of the actuation, cell placement and imaging

cally and the thickness of the polysilicon was measured using a profilometer. The theoretical spring constant was calculated as $163.36 \text{ nN}/\mu\text{m}$ using the measured dimensions. The accuracy of the calibration verifies the measured dimensions used for the theoretical spring calculation of the beam.

Sample preparation

A standard probe station was modified to accommodate the actuating, sensing, image acquisition and cell placement equipment concurrently (Fig. 5). It is crucial to create a hospitable environment on the probe station to allow the cell to adhere and remain viable for an extended period of time. A commercially available microincubator was used to house the Petri dish and chip and to maintain the cell media at 37°C .

Traditional methods for preparing chips for cell protocols require drying the chip after release and placing the chip in cell media or deionized (DI) water. The transition from air to water can damage fine structures or cause stiction of suspended beams. We have developed a novel process to avoid this problem. Prior to release, the chips are anchored to a 25 mm polystyrene Petri dish using a cyanoacrylate adhesive. The chips are then wet-etched with hydrofluoric acid directly in the Petri dish. At the completion of the etch, the acid is drained and replaced with deionized water. The chip is then allowed to soak in DI water for 12 hours. The released chip is never exposed directly to air and never allowed to dry. This technique avoids damage to the delicate structures by the surface tension of the water as reported by other groups with similar designs (Saif et al., 2003). By utilizing this novel release process, delicate structures can be fabricated that would not normally survive the transition from air to water.

After release, the chip was prepared for the experiment by draining the DI water and rinsing with phosphate-buffered saline (PBS). The Petri dish containing the chip was then

filled with a solution of $20 \mu\text{l}$ fibronectin and $780 \mu\text{l}$ of PBS and placed in an incubator for four hours.

Hamster fibroblast cells were obtained commercially and were cultured in T75 cell culture flasks inside an incubator at 37°C and 5% CO_2 -95% using a commercial media supplemented with 10% fetal bovine serum (FBS) as well as antibiotics. The cells were ready for the experiment when the monolayers reached approximately 80% of their full confluent growth. Cell suspensions were obtained by detaching cells from flasks with exchanges of buffer and enzyme solutions to cleave adhesion sites on cells. Cells were rinsed in PBS and then removed from the culture dish using a 0.025% trypsin in ethylenediaminetetraacetic acid (EDTA) solution for two minutes and then re-suspended in a cell media. The fibroblasts were centrifuged into pellet form and, once again, resuspended in fibroblast media for the experiments to a concentration of $14 \times 10^4/\text{mL}$. A drop of this solution was placed onto the chip.

Once the cells were settled on the chip but before they had an opportunity to adhere, a single cell was positioned on the platform using a commercial device that dispenses picoliter volumes of media in a controlled fashion. A standard probe tip cannot be used to position single cells. The tip can cause damage to the delicate cell membrane and the cell frequently adheres to the probe tip, making placement impossible. The picoliter dispensing instrument allows small volumes of media to be injected through a glass pipette tip ($\text{ID} = 10 \mu\text{m}$). The force of the injected media is sufficient to push a single cell onto the platform without the need to contact the cell. Once the cell is placed on the platform, it is allowed to spread and adhere to the platform. The rate at which the cell adheres varies depending upon cell type and substrate chemistry. Experimentally, the time period for the cell to adhere and spread out was found to be one to three hours.

Device fabrication

The devices were fabricated using a custom process developed utilizing the NIST fabrication facility (Fig. 6). A $1 \mu\text{m}$ low temperature oxide layer (LTO) is deposited by low pressure chemical vapor deposition (LPCVD) on single-sided n-type wafers. The thickness of the film is verified using an ellipsometer. The via and dimple etch are performed using a reactive ion etcher (RIE). Polysilicon is deposited by LPCVD to a depth of $2 \mu\text{m}$ then annealed at 1050°C for two hours. The structures are patterned and then etched using a deep reactive ion etcher (DRIE). These chips are wet etched with hydrofluoric acid after which the chips are dried in a CO_2 critical point dryer. Prototypes are evaluated and examined using a scanning electron microscope (SEM).

The custom fabrication process allows the geometry of the device to be designed to suit a variety of biological ex-

Fig. 6 Thermal wet oxide is grown on standard single-crystal-silicon wafers (B). The dimple and via etch are done using an RIE (C). Polysilicon is deposited to a depth of $2\ \mu\text{m}$ (D) and annealed. The polysilicon structures are defined using a DRIE (E). The oxide is etched away to release the structures (F)

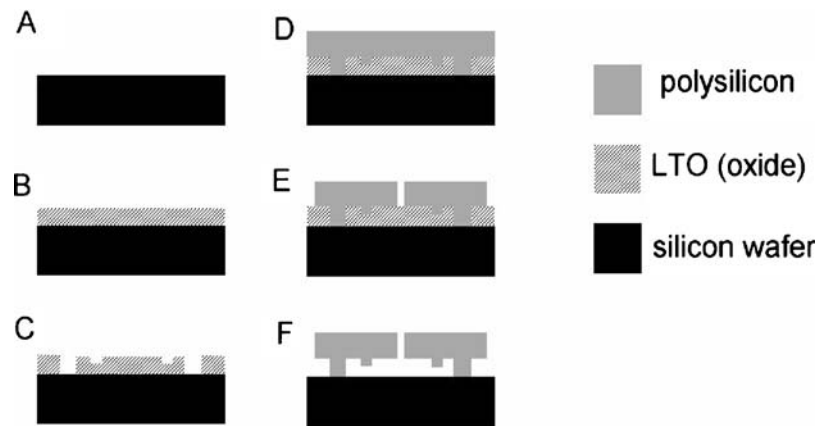
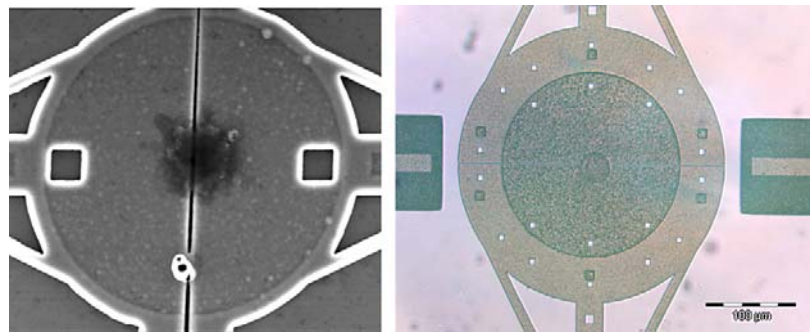


Fig. 7 A fibroblast is placed on the platform



periments. The geometry of any aspect of the device such as the actuator, sensor or cell platform can be modified for specific cell types and experimental protocols.

Results and discussion

A single fibroblast cell was placed on the cell platform using the above technique (Fig. 7) and allowed to adhere for three hours. A displacement was then applied to the cell at a rate of $400\ \text{nm/s}$ to a maximum displacement of $90\ \mu\text{m}$. The force response of the cell was measured throughout the course of the applied displacement.

The applied displacement and force on the cell were plotted versus time (Fig. 8(A)). Force is calculated using:

$$F_{\text{cell}} = k_{\text{spring}} * d_{\text{sensor}} \quad (10)$$

where k_{spring} is the spring constant for the folded-beam assembly and d_{sensor} is the displacement of the sensor half of the cell platform. Thus, the cell is strained between the two halves of the cell platform (Fig. 8(B)). The curve shows two distinct regions of the cell deformation. The first region spans from the onset of the applied displacement to approximately $92\ \text{s}$ at which point the cell begins to de-adhere. This region is linear with respect to time ($R^2 = 0.991$). Initially, several adhesion sites fail allowing the cell to relieve the associated

stress at a force of $1330\ \text{nN}$. However, as the cell is stretched further, the remaining adhesion sites begin to fail and the force drops sharply at a force of $1551\ \text{nN}$. It should also be noted that while a de-adhesion force is reported here, future designs will allow the effective area of adhesion to be quantified allowing a stress measurement to be reported.

There is some uncertainty in the force measurement due to several sources. The first is the measurement of the displacement. As stated earlier, the estimated resolution of displacement is $50\ \text{nm}$. We arrived at this number by tracking a stationary feature over the course of the experiment. The algorithm perceived the stationary object to move a maximum of $50\ \text{nm}$ from frame to frame. This is primarily caused by the subtle variations in contrast from image to image. The calibration of the images using a calibration slide also introduces errors. We estimate the calibration of the objective to be in error by approximately 2% based on known lengths. The second source of uncertainty comes from the AFM cantilever. Tortonese and Maruyama (1977) state the error in the calibration of the cantilever tip to be 3.3% and the calibration of the spring was in error with the theory by almost 8% . Thus, the calibration of the springs has the same error Tortonese and Maruyama report. The mounting of the AFM cantilever at 12.5° can be off by several degrees. However, the error introduced by this is minimal. Based on the above, we estimate the relative standard uncertainty to be approximately 10% .

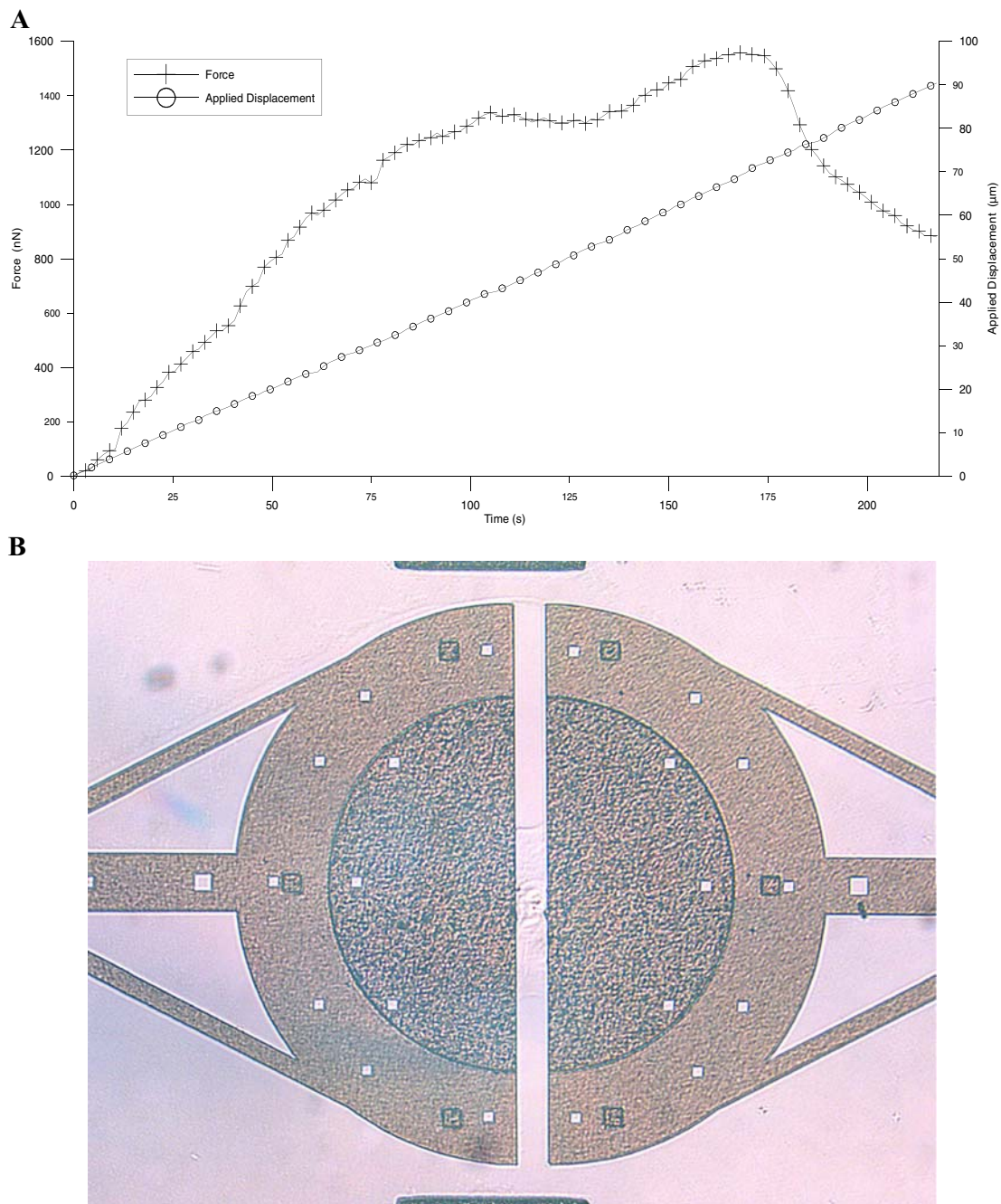


Fig. 8 Force exerted on a fibroblast cell and the applied displacement as a function of time (A). Fibroblast cell being stretched during the experiment (B)

The linear region of the force vs. time curve is typical for cells under stretch. Saif et al. (2002, 2003) reported a linear response of fibroblasts when exposed to stretch from a silicon cantilever. However, the de-adhesion force is high compared with other approaches. This can be attributed to several factors. The force being applied to the adherent cell is a shear force. Other de-adhesion studies applying a shearing force to adherent cells using an AFM have indicated forces as high as 400 nN (Missirlis and Spiliotis, 2002). The surface

roughness of the cell platform in the design presented here is high compared with glass cover slips on which many de-adhesion experiments are performed. Surface roughness and the addition of a fibronectin protein layer have been shown to increase de-adhesion forces (Dean et al., 1995; Degasne et al., 1999). When these effects are combined, the high de-adhesion strength can be explained. Further investigations using a large sample size can be performed to verify these data.

While a simple displacement was applied as a demonstration, the applicability of a device such as this to single cell experiments is broad. Many parameters can be investigated using this device. De-adhesion experiments involving varying surface roughness, substrate material and extra cellular matrix (ECM) chemistries can be studied to verify the presented data. Strain rate and displacements can be varied to study force response from a variety of cell types as well as viscoelastic response of single cells.

Conclusion

A novel, microfabricated device for single-cell mechanical measurements is demonstrated. The device was fabricated using a single-layer polysilicon process. The device consists of a circular cell platform on which a single cell is placed. A displacement is applied to the cell and the force on the cell can be calculated.

Several novel techniques were developed to allow the device to work as designed. A release technique has been developed to allow for fine spring structures to be fabricated and increase the resolution of the force measurements. A cell placement protocol was developed to allow the placement of single cells on the cell platform. This technique is applicable to a variety of cell types and devices requiring accurate placement of single cells.

The device is demonstrated by applying strain to an adherent fibroblast until the cell begins to de-adhere. A de-adhesion force of 1551 nN is reported. The high force required to de-adhere the cell is a result of the surface roughness of the platform, the shear force applied to the cell and the protein layer used to encourage adhesion.

The device is broadly applicable to a variety of cellular experiments including static de-adhesion experiments as well as cyclic strain experiments. Future designs will integrate a transparent substrate that will allow the imaging of the cell in real-time. This will facilitate the correlation of mechanical forces with cellular morphology.

Acknowledgments The authors would like to thank Peter L. Jones for valuable input on BioMEMS and cellular mechanics ideas.

References

- K.M. Ainslie, J.S. Garanich, R.O. Dull, and J.M. Tarbell, *J. Appl. Physiol.* **98**, 242 (2005).
 F.J. Alenghat, B. Fabry, K.Y. Tsai, W.H. Goldmann, and D.E. Ingber, *Biochem. Biophys. Res. Commun.* **277**, 93 (2000).
 J. Chen, B. Fabry, E.L. Schiffrin, and N. Wang, *Am. J. Physiol. Cell. Physiol.* **280**, C1475 (2001).
 M.E. Chicurel, C.S. Chen, and D.E. Ingber, *Curr. Opin. Cell Biol.* **10**, 232 (1998).

- J.W. Dean, K.C. Culbertson, and A.M. D'Angelo, *Int. J. Oral. Maxillofac. Implants* **10**, 721 (1995).
 I. Degasne, M.F. Basl, †, V. Demais, G. Hur, M. Lesourd, B. Grolleau, L. Mercier, and D. Chappard, *Calcif. Tissue Int.* **64**, 499 (1999).
 N. Desprat, A. Richert, J. Simeon, and A. Asnacios, *Biophysical. J.* **88**, 2224 (2005).
 F. Di Palma, M. Douet, C. Boachon, A. Guignandon, S. Peyroche, B. Forest, C. Alexandre, A. Chamson, and A. Rattner, *Biomaterials* **24**, 3139 (2003).
 E. Evans and A. Yeung, *Biophysical. J.* **56**, 151 (1989).
 E.A. Evans and R.M. Hochmuth, *Biophys. J.* **16**, 1 (1976).
 B. Fabry, G.N. Maksym, J.P. Butler, M. Glogauer, D. Navajas, and J.J. Fredberg, *Phys. Rev. Lett.* **87**, 148102 (2001).
 B. Fabry, G.N. Maksym, J.P. Butler, M. Glogauer, D. Navajas, N.A. Taback, E.J. Millet, and J.J. Fredberg, *Phys. Rev. E. Stat. Nonlin. Soft Matter. Phys.* **68**, 041914 (2003).
 E.L. Florin, V.T. Moy, and H.E. Gaub, *Science* **264**, 415 (1994).
 Y.C. Fung and S.Q. Liu, *J. Biomech. Eng.* **115**, 1 (1993).
 R.M. Hochmuth, *Scand. J. Clin. Lab. Invest. Suppl.* **156**, 63 (1981).
 R.M. Hochmuth and R.E. Waugh, *Annu. Rev. Physiol.* **49**, 209 (1987).
 K. Hyonchol, H. Arakawa, T. Osada, and A. Ikai, *Colloids Surf. B: Biointerfaces* **25**, 33 (2002).
 A. Ignatius, H. Blessing, A. Liedert, D. Kaspar, L. Kreja, B. Friemert, and L. Claes, *Orthopade* **33**, 1386 (2004).
 P.A. Janmey, *Physiological. Rev.* **78**, 763 (1998).
 T.J. Lardner and R.R. Archer 262 (1994).
 C.M. Lo, M. Glogauer, M. Rossi, and J. Ferrier, *Eur. Biophys. J.* **27**, 9 (1998).
 A. Maniotis, C. Chen, and D. Ingber, *Proceeding of the National Acad. Sci.* **94**, 849 (1997).
 A.B. Mathur, A.M. Collinsworth, W.M. Reichert, W.E. Kraus, and G.A. Truskey, *J. Biomech.* **34**, 1545 (2001).
 A. Minajeva, M. Kulke, J.M. Fernandez, and W.A. Linke, *Biophys. J.* **80**, 1442 (2001).
 Y.F. Missirlis and A.D. Spiliotis, *Biomol. Eng.* **19**, 287 (2002).
 M. Moretti, A. Prina-Mello, A.J. Reid, V. Barron, and P.J. Prendergast, *J. Mater. Sci. Mater. Med.* **15**, 1159 (2004).
 J.S. Park, J.S. Chu, C. Cheng, F. Chen, D. Chen, and S. Li, *Biotechnol. Bioeng.* **88**, 359 (2004).
 N.P. Rhodes, A.P. Shortland, A. Rattray, and D.F. Williams, *J. Mater. Sci. Mater. Med.* **9**, 767 (1998).
 T. Saif, C.R. Sager, and S. Coyer, *Ann. Biomed. Eng.* **31**, 950 (2003).
 T. Saif, C. Sager, and S. Coyer, *American Society of Mechanical Engineers, Micro-Electromechanical Systems Division Publication (MEMS)*, 591 (2002).
 G.W. Schmid-Schonbein, K.L. Sung, H. Tozeren, R. Skalak, and S. Chien, *Biophys. J.* **36**, 243 (1981).
 A. Soghomonians, A.I. Barakat, T.L. Thirkill, and G.C. Douglas, *Biol. Reprod.* (2005).
 K. Svoboda and S.M. Block, *Ann. Rev. Biophys. Biomol. Struct.* **23**, 247 (1994).
 O. Thoumine and A. Ott, *J. Cell Sci.* **110**(Pt 17), 2109 (1997).
 M. Tortonesi and N. Maruyama, *Micromachining Imaging* **3009**, 53 (1997).
 N. Wang, J.P. Butler, and D.E. Ingber, *Science* **260**, 1124 (1993).
 S. Yamada, D. Wirtz, and S.C. Kuo, *Biophys. J.* **78**, 1736 (2000).
 A. Yamamoto, S. Mishima, N. Maruyama, and M. Sumita, *Biomaterials* **19**, 871 (1998).
 S. Yang and T. Saif, *Exp. Cell Res.* **305**, 42 (2005).
 K.S. Zaner and P.A. Valberg, *J. Cell Biol.* **109**, 2233 (1989).